Title
Distinct Tissue Mineral Density in Plate- and Rod-like Trabeculae of Human Trabecular Bone

Journal
Journal of Bone and Mineral Research, 30(9)

ISSN
0884-0431

Authors
Wang, Ji
Kazakia, Galateia J
Zhou, Bin
et al.

Publication Date
2015-09-01

DOI
10.1002/jbmr.2498

Peer reviewed

HHS Public Access

Author manuscript

J Bone Miner Res. Author manuscript; available in PMC 2016 September 01.

Published in final edited form as:

J Bone Miner Res. 2015 September ; 30(9): 1641–1650. doi:10.1002/jbmr.2498.

Distinct tissue mineral density in plate and rod-like trabeculae of human trabecular bone

Ji Wang[1], **Galateia J. Kazakia**[2], **Bin Zhou**[1], **X. Tony Shi**[1], and **X. Edward Guo**[1]

Ji Wang: jw2857@columbia.edu; Galateia J. Kazakia: Galateia.Kazakia@ucsf.edu; Bin Zhou: bz2159@columbia.edu; X. Tony Shi: xshi3@alumni.nd.edu; X. Edward Guo: exg1@columbia.edu

[1]Bone Bioengineering Laboratory, Department of Biomedical Engineering, Columbia University, New York, New York, U.S.A.

[2]Musculoskeletal Quantitative Imaging Research Group, Department of Radiology and Biomedical Imaging, University of California, San Francisco, San Francisco, CA, USA.

Abstract

Trabecular bone quality includes both microstructural and intrinsic tissue mineralization properties. However, the tissue mineralization in individual trabeculae of different trabecular types and orientations has not yet been investigated. The aim of this study was to develop an individual trabecula mineralization (ITM) analysis technique to determine tissue mineral density (TMD) distributions in plate- and rod-like trabeculae, respectively, and to compare the TMD of trabeculae along various orientations in μCT images of trabecular bone samples from the femoral neck, greater trochanter, and proximal tibia. ITM analyses indicated that trabecular plates, on average, had significantly higher TMD than trabecular rods. In addition, the distribution of TMD in trabecular plates depended on trabecular orientation with the lowest TMD in longitudinal plates and the highest TMD in transverse plates. Conversely, there was a relatively uniform distribution of TMD among trabecular rods, with respect to trabecular orientation. Further analyses of TMD distribution revealed that trabecular plates had higher mean and peak TMD, whereas trabecular rods had a wider TMD distribution and a larger portion of low mineralized trabeculae. Comparison of apparent Young's moduli derived from micro finite element models with and without heterogeneous TMD demonstrated that heterogeneous TMD in trabecular plates had a significant influence on the elastic mechanical property of trabecular bone. In conclusion, this study revealed differences in TMD between plate and rod-like trabeculae and among various trabecular orientations. The observation of less mineralized longitudinal trabecular plates suggests interesting implications of these load-bearing plates in bone remodeling. The newly developed ITM analysis can be a valuable technique to assess the influence of metabolic bone diseases and their pharmaceutical treatments on not only microstructure of trabecular bone, but also the microarchitectural heterogeneity of tissue mineralization.

Correspondence to: X. Edward Guo, `exg1@columbia.edu`.

The authors have nothing to disclose

Additional Supporting Information may be found in the online version of this article.

Authors' roles: Study design: XEG and GJK. Data collection: JW and GJK. ITM analysis: JW. Finite element analysis: BZ and XTS. Data interpretation: JW, GJK, and XEG. Drafting manuscript: JW. Revising manuscript content and approving final version of manuscript: all authors.

Keywords

Tissue Mineral Density; Individual Trabecula Mineralization; Individual Trabecula Segmentation; Micro Computed Tomography

Introduction

Tissue mineral density (TMD) and its heterogeneous distribution are key determinants of the intrinsic mechanical properties of trabecular bone tissue [1,2]. The nonuniform TMD in trabecular bone tissue results from frequent bone remodeling and dynamic mineralization kinetics in newly formed bone packets. Normal healthy adults have a characteristic TMD distribution regardless of gender, age and race. Many bone metabolic diseases, e.g., osteoporosis and osteomalacia, are associated with distinct deviations from the reference TMD distribution of healthy individuals [3,4]. Additionally, patients with fragility fractures at the hip and spine have more heterogeneous bone mineralization than the nonfracture control subjects [5–7]. These findings suggest basic science and diagnostic value for evaluating the distribution of TMD; however, knowledge is lacking regarding factors that contribute to the heterogeneity of TMD. For instance, bone mineralization has not yet been investigated on the individual trabecular level. In addition, we do not know how individual trabecular TMD varies with trabecular types and orientations.

Trabecular bone microstructure is an important determinant for bone strength and fragility that is independent of areal bone mineral density measurement by dual-energy X-ray absorptiometry (DXA) [8,9]. Individual trabecula segmentation (ITS)-based morphological analysis, which segments trabecular microstructure into individual trabecular plates and rods, has demonstrated that trabecular plates and rods of different orientations have varying impact on the mechanical properties and failure mechanisms of trabecular bone [10–14]. Based on microstructural differences between trabecular plates and rods, we hypothesize that plate-like and rod-like trabeculae also differ in TMD, and trabeculae of different orientations have different TMD.

By combining high-resolution three-dimensional (3D) micro computed tomography (μCT) imaging and ITS analysis, we developed a new volumetric mineralization analysis technique, individual trabecula mineralization (ITM), which provides detailed and direct measurements of TMD of individual trabecular plates and rods. In brief, the gray levels of a μCT voxel represent the mineral density of the corresponding volume of bone tissue, and trabecular microstructure obtained from thresholded images can be further segmented into individual trabecular plates and rods by ITS. Considering the beam hardening effect introduced by polychromatic x-ray source in the μCT system, the ITM technique using μCT was first compared to that based on synchrotron radiation μCT (SRμCT), the gold standard for 3D TMD evaluation without any beam hardening. Then, we used the newly developed ITM technique to (1) quantify the TMD of individual trabeculae in human trabecular bone; (2) compare the TMD distributions of plate- and rod-like trabeculae; (3) establish the relationship between TMD and trabecular orientation; (4) evaluate the influence of TMD variation on apparent Young's modulus of trabecular bone.

Materials and Methods

Validation Set

In order to verify the ITM measurements, trabecular bone samples were prepared at the University of California at San Francisco and imaged by both SRμCT and μCT as described in Kazakia et al.. Trabecular bone cores (8 mm diameter, 4 mm length) were obtained from the femoral head (n=5), vertebral body (n=5), and proximal tibia (n=4). SRμCT imaging was performed on a beamline X2B of the National Synchrotron Light Source (Brookhaven National Laboratory, Upton, NY). 3D SRμCT images of trabecular bone samples were reconstructed at an isotropic voxel size of 7.50 μm. μCT imaging was performed on a μCT 40 (Scanco Medical AG, Switzerland) combined with two beam hardening correction (BHC) factors derived from the polynomial attenuation profiles of two wedge phantoms composed of a hydroxyapatite (HA)-resin mixture of 200 mg HA/cm^3 and 1200 mg HA/cm^3, respectively. μCT images were reconstructed at an isotropic voxel size of 8 μm. A Gaussian filter along with site- and modality-specific threshold values were applied. A HA rod density calibration phantom was scanned under the same conditions as the trabecular bone samples to convert attenuation levels to HA concentrations for the SRμCT data, μCT data with 200 mg HA/cm^3 BHC, and μCT data with 1200 mg HA/cm^3 BHC. Kazakia et al.[15] has reported this data set and compared TMD measurements of the SRμCT and μCT images.

Experimental Set

Sixty-three cylindrical (8mm diameter, 20 mm length) human trabecular bone samples were obtained from the proximal tibia (PT, n=22), greater trochanter (GT, n=21), and femoral neck (FN, n=20) at Columbia University (Table 1). The subjects (n=26, 19 male and 7 female, 69±12 years) were screened to exclude history of metabolic bone diseases or bone cancers. X-ray radiographs were taken to ensure no evidence of damage, fracture, or other bone pathologies. Trabecular bone cores were drilled along the principle loading direction following a previously reported protocol [16]. To ensure that the longitudinal axis of the bone core was aligned along the primary trabecular orientation, X-ray radiographs were taken on two orthogonal planes parallel with the longitudinal axis. Any sample with an angle between the trabecular orientation and the longitudinal axis larger than 10° was excluded from this study. Samples were wrapped with wet gauze in airtight plastic bags and stored at −20°C when not being processed. Images of the central gauge length of 8 mm were obtained by μCT (VivaCT 40, Scanco Medical AG, Switzerland) at an isotropic voxel size of 15 μm with a source potential of 55 kV and tube current of 109μA. To minimize the beam hardening effect, a standard aluminum filter was installed in the μCT scanner, and a voltage- and scanner- specific BHC algorithm derived from a wedge phantom of 200 mg HA/cm^3 density was implemented [17]. Gaussian filter and anatomic site-specific threshold values were applied to segment grayscale images into binary images composed of bone and marrow. We have reported the bone morphology and mechanics data of these specimens [13,18]. Furthermore, the original grayscale value of each voxel, representing the attenuation coefficient, was converted to HA concentration using a linear regression derived by imaging a calibration phantom containing rods of HA-resin mixtures (0, 100, 200, 400, and 800 mg HA/cm^3). Given that the peripheral regions of the trabecular bone cores were likely to be

affected by cupping artifact, the central 5×5×5 mm^3 cubic sub-volume of each image was extracted for subsequent ITM analysis.

Individual Trabecula Mineralization (ITM) Analysis

Grayscale images containing volumetric bone mineral densities (in mg HA/cm^3) and binary images representing trabecular microstructure were both imported into ITM analysis (Fig. 1). By ITS, trabecular bone microstructure was decomposed into individual trabecular plates and rods [10,19,20]. Briefly, through an iterative thinning process, a surface and curve skeleton of the trabecular bone microstructure was extracted with its topology and morphology fully preserved [20]. Then, the entire skeleton was decomposed into individual trabecular skeletons with each voxel uniquely classified as either a plate or a rod type based on digital topological classification [19]. The segmented skeleton was then returned to the original volume as a collection of individual trabecular plates and rods labeled with unique identification numbers. To quantify TMD of each individual trabecula, the segmented trabecular plate and rod microstructure was mapped to the original grayscale image. On the single voxel level, the volumetric mineral density was determined from the grayscale value by the linear regression derived from the HA calibration phantom scan, and the microstructural type was classified as either trabecular plate or rod. Individual trabecula TMD was defined as the average TMD of all the voxels that belonged to this trabecula. Additionally, the orientation of individual trabecular plates or rods was determined with reference to the principal trabecular direction of the bone sample. For a trabecular plate, angle Φ was defined as the angle between the normal vector of the plate and the longitudinal axis. For a trabecular rod, angle Φ was defined as the angle between the direction of the rod and the longitudinal axis. Trabecular orientations were categorized into longitudinal (angle Φ 60°~90° for plates and 0°~ 30° for rods), oblique (angle Φ 30°~60° for plates and rods), and transverse (angle Φ 0°~ 30° for plates and 60°~90° for rods).

TMD Distributions in Trabecular Plates and Rods

A histogram of TMD distribution in individual trabecular plates and rods was plotted. The following parameters were defined to characterize a TMD distribution: the average TMD of plate- and rod-like trabeculae ($pTMD_{MEAN}$, $rTMD_{MEAN}$), the most frequent TMD of trabecular plates and rods ($pTMD_{PEAK}$, $rTMD_{PEAK}$), the width of distributions in trabecular plates and rods at half maximum frequency ($pTMD_{WIDTH}$, $rTMD_{WIDTH}$), the percentage of trabecular plates and rods whose TMD was lower than the 5^{th} percentile of the overall distribution ($pTMD_{LOW}$, $rTMD_{LOW}$), and the percentage of trabecular plates and rods which were mineralized above the 95^{th} percentile of the overall distribution ($pTMD_{HIGH}$, $rTMD_{HIGH}$). The low and high mineralization cutoff values were determined based on the pooled TMD distribution at each of the anatomic sites in the validation set and experimental set.

Micro Finite Element Analysis

Four micro finite element (μFE) models were generated for each specimen using different bone tissue properties: (1) a homogeneous model with a constant tissue modulus as determined by the average TMD of the specimens; (2) a heterogeneous model with tissue modulus as determined by volumetric TMD; (3) a plate-heterogeneous model with tissue

modulus for trabecular plates determined by individual pTMD and a constant homogeneous tissue modulus for trabecular rods as determined by the average rTMD; (4) a rod-heterogeneous model with tissue modulus for trabecular rods determined by individual rTMD and a constant homogeneous tissue modulus for trabecular plates as determined by the average pTMD. Trabecular bone tissue was modeled as an isotropic, linear elastic material with a Poisson's ratio of 0.3[21]. For the heterogeneous models, 32 material properties were adopted based on the linear correlation between TMD and tissue modulus [21,22]. For the homogeneous model, the elastic modulus was assumed according to the average TMD based on the linear relation. An eight-node brick element was constructed for each μCT image voxel. μFE analysis simulating a compression test along the longitudinal direction of the trabecular bone sample was performed, and apparent Young's modulus was derived. To determine the influence of TMD variation on the apparent Young's modulus, we compared the apparent Young's moduli predicted by the homogeneous model, plate-heterogeneous model, and rod-heterogeneous model with reference to the heterogeneous model, which accounts for heterogeneity of TMD for both trabecular plates and rods.

Statistical Analysis

Statistical analyses were conducted with NCSS (NCSS Statistical Software, Kaysville, Utah). Paired Student's *t* test was applied to compare the TMD distribution parameters of plate- and rod-like trabeculae. Two-sided p value <0.05 was considered to indicate statistically significant. Differences between trabecular plate and rod TMD distributions were further assessed by a Kolmogorov-Smirnov test. Bland-Altman plots were used to show the disparity between the heterogeneous model and the homogeneous, plate-heterogeneous, or rod-heterogeneous model. The relative difference between two methods (difference/average) was plotted versus their average.

Results

TMD Distributions in the Validation Set

Compared to trabecular plates, trabecular rod TMD had a wider distribution and a bigger tail in the low TMD range (Fig. 2 A~C). Differences between TMD distributions in trabecular plates and rods were more pronounced in the SRμCT data, while a similar pattern was observed in the μCT data with 200 BHC and 1200 mg HA/cm^3 BHC. Statistically, the two-sample Kolmogorov-Smirnov test suggested that TMD distributions in trabecular plates and rods were distinct from each other, based on comparing the cumulative distribution functions of two data sets. TMD values measured by SRμCT were significantly higher than μCT-based TMD values, as shown in Fig. 2 D~F. The relatively larger underestimation of TMD by the 200 mg HA/cm^3 beam hardening correction led to further discrepancy between μCT and SRμCT data. Kazakia et al. [15] reported the regressions between μCT and SRμCT TMD measurements of this exact validation data set. Strong correlations (R^2=0.78~0.99) were found between TMD values calculated by SRμCT and μCT using two beam hardening correction algorithms. Regressions of individual trabecula TMD measurements in our current study resulted in similar correlations (R^2=0.71~0.95) between SRμCT and μCT data (Fig. 2 G~I). TMD distribution parameters were derived for each specimen and summarized

in Table 2. In the SRμCT data, $rTMD_{MEAN}$ and $rTMD_{PEAK}$ were significantly lower than $pTMD_{MEAN}$ and $pTMD_{PEAK}$ by 3% and 2%, respectively. $rTMD_{WIDTH}$ was 30% higher than $pTMD_{WIDTH}$. $rTMD_{LOW}$ was 150% higher than $pTMD_{LOW}$, which was the most striking difference between two TMD distributions. Furthermore, lower $rTMD_{MEAN}$ and higher $rTMD_{LOW}$ were consistent in the three data sets of SRμCT, μCT with 200 and 1200 mg HA/cm^3 BHC.

TMD Distributions in the Experimental Set

As the validation set demonstrated substantial differences between the TMD distributions in trabecular plates and rods, the experimental set from FN, PT and GT was used to establish the characteristic TMD distributions in individual trabecular plates and rods of different orientations (Fig. 3). Trabecular plate and rod TMD distributions in the experimental set agreed with what we observed in the validation set. More specifically, trabecular rod TMD distribution shifted towards lower TMD relative to trabecular plate TMD distribution with a wider band and a heavier tail in the low TMD range. Distribution indexes showed that $rTMD_{MEAN}$ and $rTMD_{PEAK}$ were lower than $pTMD_{MEAN}$ and $pTMD_{PEAK}$ by 2.3% and 1.4%, respectively. $rTMD_{WIDTH}$ was 8.8% higher than $pTMD_{WIDTH}$, and $rTMD_{LOW}$ was 140.8% higher than $pTMD_{LOW}$. Lower $rTMD_{MEAN}$ and higher $rTMD_{LOW}$ relative to $pTMD_{MEAN}$ and $pTMD_{LOW}$ were found consistently at FN, GT, and PT (Table 3). We observed that trabecular bone at FN had higher TMD and higher BV/TV than PT and GT. We did not observe a difference in TMD between male and female subjects. Finally, trabecular plate and rod TMD did not increase with age of the subjects ($p=0.17$); however, this observation could be limited by the number of specimens in this study.

TMD of Individual Trabeculae along Different Orientations

In the experimental set, we observed that TMD of individual trabecular plates increased from the longitudinal to the transverse direction, namely longitudinal trabecular plates had lower TMD than oblique and transverse plates (Fig. 4). Such orientation-wise TMD variation in trabecular plates was consistent across all tested anatomic sites. Conversely, trabecular rod TMD was relatively uniform along different trabecular orientations. Trabecular bone at FN had a higher proportion of transverse trabeculae (14%) and a lower proportion of axially aligned trabeculae (65%) compared with GT and PT ($p<0.05$), which had 11% and 8% transverse trabeculae, and 72% and 80% axial trabeculae ($p<0.05$), respectively.

Effect of TMD Variation on Apparent Young's Modulus Prediction

Apparent Young's moduli of trabecular bone predicted by homogeneous models, plate-heterogeneous models, and rod-heterogeneous models were all highly correlated with the results of heterogeneous models with R^2 close to 1. Nevertheless, there was a −5% to 12% relative difference in apparent Young's modulus calculated by the homogeneous model as compared with the heterogeneous model (Fig. 5). The plate-heterogeneous model yielded an apparent Young's moduli closer to the heterogeneous model than the rod-heterogeneous model, ±3% compared to −5%~10% difference. The discrepancies between these models were more pronounced in specimens with lower modulus, presumably specimens at PT and GT with lower BV/TV.

Discussion

In this study, we developed an ITM technique, which integrated bone mineralization assessment and trabecular microstructure segmentation, to investigate heterogeneity of TMD associated with trabecular microstructural types and orientations. ITM analysis demonstrated that plate-like trabeculae, on average, had higher TMD than rod-like trabeculae across the anatomic sites of FN, GT and PT. Furthermore, trabecular plate TMD varied among different orientations, showing a significant increase of TMD from the longitudinal plates to the transverse ones. In contrast, trabecular rod TMD had lower average TMD with a wider distribution, and showed little variation along different trabecular orientations.

ITM assessment was first tested on SRμCT images, in the absence of beam hardening effect, and then compared to the results from μCT images of the same trabecular bone samples after BHC. Higher average TMD in trabecular plates than rods was observed in both SRμCT and μCT data. In fact, the difference between trabecular plate and rod TMD distributions was more pronounced in the SRμCT data. These observations verified distinct trabecular plate and rod TMD distributions in the absence of beam hardening effect, and provided important reference to estimate the deviation of μCT-based ITM assessment compared to SRμCT-based results.

ITM analysis revealed that trabecular plates had a significantly higher average TMD than trabecular rods, suggesting a lower bone turnover in trabecular plates which might result from lower surface to volume ratio in trabecular plates. The proportion of trabecular rods with low TMD, below the 5^{th} percentile of the overall TMD distribution, was twice to five times as that of trabecular plates. Also, trabecular rod TMD tended to be more heterogeneous, suggested by a wider distribution. Similarly, using qBEI, Busse et al. observed elevated mineral density distribution in plate-like trabeculae compared to rod-like trabeculae in osteoporotic vertebral bone [23]. Furthermore, in this study, we observed lower TMD in the longitudinal trabecular plates than the transverse ones, however trabecular rod TMD did not vary with trabecular orientation. It is worth noting that specimens in the experimental set were scanned with the transverse plates parallel to the x-ray beam path, so transverse plates were likely more influenced by beam hardening effect and underestimated in TMD assessment. In spite of this, transverse plates were found to be higher mineralized than longitudinal plates across different anatomic sites. Therefore, our finding was unlikely caused by beam hardening artifact. Additionally, we observed such heterogeneity in plate TMD with orientation in the SRμCT validation set of vertebral specimens, which were harvested with the long axis of the bone core aligned with the superior-inferior direction (the other specimens not controlled in orientation). Lower TMD in the longitudinal trabecular plates, which account for the majority of trabecular plate volume and the predominant load-bearing elements in trabecular network [9,10,12,24], might suggest relatively more proactive bone remodeling in those load-bearing trabeculae in response to physiological mechanical loading. The relatively lower TMD in trabecular rods, in general, might suggest active and constant remodeling process in trabecular rods, making them more vulnerable for osteoporotic loss. These new observations in trabecular plate and rod ITM distributions

suggest interesting interactions that may inform future directions in bone remodeling studies.

Comparison of heterogeneous and homogeneous models demonstrated difference in apparent Young's modulus of trabecular bone resulted from incorporation of specimen-specific heterogeneous TMD into μFE analysis. Similarly, Gross et al.[25] reported overestimation of elastic properties of trabecular bone by homogeneous SRμCT-based FE models as compared with heterogeneous models. ITM analysis allows selectively taking into account TMD variation of trabecular plates or rods. Better agreement between the plate-heterogeneous and heterogeneous models suggested greater impact of TMD variation in trabecular plates on the apparent elastic property of trabecular bone. It is interesting that the major discrepancies between homogeneous and heterogeneous models concentrated in the low BV/TV regime, suggesting that ITM based TMD evaluations may have important clinical applications in the accurate assessment of biomechanical bone quality in osteoporosis and in response to clinical interventions. This quantitative study indicates only moderate contributions of trabecular TMD heterogeneities to mechanical properties of human trabecular bone. The roles of the anisotropic and heterogeneous individual trabecular plate and rod TMD-based tissue properties on the mechanical behavior of human trabecular bone remain to be quantified. In addition, it will be interesting to study trabecular plate and rod TMD distributions in metabolic bone diseases known to affect TMD, such as chronic kidney disease or diabetes [26,27], and changes to bone quality in response to anabolic treatments, such as parathyroid hormone or antibody against sclerostin [28,29].

There are certain limitations associated with the present study. First, ITM assessment based on μCT images is inevitably subjected to partial volume effect caused by voxels on the bone surface containing half bone and half marrow. In the case of high-resolution μCT images, e.g., 15 μm voxel size used in this study, the influence introduced by partial volume effect should be minor. Furthermore, we compared ITM results with and without the bone surface voxels removed (data not shown). Except for elevated TMD of all trabeculae, we observed no change in major observations. As μCT is inherently affiliated with partial volume and beam hardening effects, ITM analysis based on μCT requires a necessary beam hardening correction, high image resolution, special caution with the sample geometry and porosity, as well as large enough sample collection to draw sound conclusions. Our repeated measurements using μCT at 15 μm indicated the high precision of the ITM technique and the influence of voxel size (15 μm compared to 30 μm) seemed to be minor (See Appendix and Tables S1 and S2). This study focused on assessment of TMD heterogeneity associated with trabecular type and orientation. Future work combining ITM analysis and bone histomorphometry may provide additional insights into individual trabecula TMD changes in relation to bone remodeling events and help explain the development of trabecular bone anisotropy.

In conclusion, this study provided direct evidence for distinct TMD distributions in plate- and rod-like trabeculae of human trabecular bone. The ITM analysis enabled evaluating the TMD of individual trabeculae for particular research interests and investigating the interaction between tissue mineralization and trabecular microstructure. By categorizing trabeculae by trabecular type and orientation, this study demonstrated higher TMD in

trabecular plates relative to rods, and higher TMD in trabecular plates along the transverse direction relative to the longitudinal direction. Since both trabecular microstructure and tissue property are important indicators for bone quality, the ITM approach will be a valuable tool to improve our understanding of bone fragility from an integrated perspective.

Acknowledgements

This work was partially supported by grants from National Institutes of Health (AR051376, AR058004, AR056734). Computational resources were made available through the National Science Foundation via XSEDE (grant TG-ECS120003). The author, Ji Wang, is supported by the Howard Hughes Medical Institute International Student Research Fellowship.

Reference

1. Rho JY, Zioupos P, Currey JD, Pharr GM. Variations in the individual thick lamellar properties within osteons by nanoindentation. Bone. 1999; 25(3):295–300. [PubMed: 10495133]
2. Jaasma MJ, Bayraktar HH, Niebur GL, Keaveny TM. Biomechanical effects of intraspecimen variations in tissue modulus for trabecular bone. Journal of Biomechanics. 2002; 35(2):237–246. [PubMed: 11784542]
3. Roschger P, Gupta HS, Berzlanovich A, Ittner G, Dempster DW, Fratzl P, Cosman F, Parisien M, Lindsay R, Nieves JW, Klaushofer K. Constant mineralization density distribution in cancellous human bone. Bone. 2003; 32(3):316–323. [PubMed: 12667560]
4. Roschger P, Paschalis EP, Fratzl P, Klaushofer K. Bone mineralization density distribution in health and disease. Bone. 2008; 42(3):456–466. [PubMed: 18096457]
5. Loveridge N, Power J, Reeve J, Boyde A. Bone mineralization density and femoral neck fragility. Bone. 2004; 35(4):929–941. [PubMed: 15454100]
6. Ciarelli TE, Fyhrie DP, Parfitt AM. Effects of vertebral bone fragility and bone formation rate on the mineralization levels of cancellous bone from white females. Bone. 2003; 32(3):311–315. [PubMed: 12667559]
7. Seitz S, Koehne T, Ries C, De Novo Oliveira A, Barvencik F, Busse B, Eulenburg C, Schinke T, Puschel K, Rueger JM, Amling M, Pogoda P. Impaired bone mineralization accompanied by low vitamin D and secondary hyperparathyroidism in patients with femoral neck fracture. Osteoporosis international : a journal established as result of cooperation between the European Foundation for Osteoporosis and the National Osteoporosis Foundation of the USA. 2013; 24(2):641–649.
8. Sornay-Rendu E, Boutroy S, Munoz F, Delmas PD. Alterations of cortical and trabecular architecture are associated with fractures in postmenopausal women, partially independent of decreased BMD measured by DXA: the OFELY study. J Bone Miner Res. 2007; 22(3):425–433. [PubMed: 17181395]
9. Liu XS, Stein EM, Zhou B, Zhang CA, Nickolas TL, Cohen A, Thomas V, McMahon DJ, Cosman F, Nieves J, Shane E, Guo XE. Individual trabecula segmentation (ITS)-based morphological analyses and microfinite element analysis of HR-pQCT images discriminate postmenopausal fragility fractures independent of DXA measurements. Journal of bone and mineral research : the official journal of the American Society for Bone and Mineral Research. 2012; 27(2):263–272.
10. Liu XS, Sajda P, Saha PK, Wehrli FW, Bevill G, Keaveny TM, Guo XE. Complete Volumetric Decomposition of Individual Trabecular Plates and Rods and Its Morphological Correlations With Anisotropic Elastic Moduli in Human Trabecular Bone. Journal of Bone and Mineral Research. 2008; 23(2):223–235. [PubMed: 17907921]
11. Liu XS, Sajda P, Saha PK, Wehrli FW, Guo XE. Quantification of the Roles of Trabecular Microarchitecture and Trabecular Type in Determining the Elastic Modulus of Human Trabecular Bone. Journal of Bone and Mineral Research. 2006; 21(10):1608–1617. [PubMed: 16995816]
12. Liu XS, Walker MD, McMahon DJ, Udesky J, Liu G, Bilezikian JP, Guo XE. Better skeletal microstructure confers greater mechanical advantages in Chinese-American women versus white women. Journal of bone and mineral research : the official journal of the American Society for Bone and Mineral Research. 2011; 26(8):1783–1792.

13. Wang J, Zhou B, Liu XS, Fields AJ, Sanyal A, Shi X, Adams M, Keaveny TM, Guo XE. Trabecular plates and rods determine elastic modulus and yield strength of human trabecular bone. Bone. 2015; 72:71–80. [PubMed: 25460571]
14. Liu XS, Wang J, Zhou B, Stein E, Shi X, Adams M, Shane E, Guo XE. Fast trabecular bone strength predictions of HR-pQCT and individual trabeculae segmentation-based plate and rod finite element model discriminate postmenopausal vertebral fractures. Journal of bone and mineral research : the official journal of the American Society for Bone and Mineral Research. 2013; 28(7):1666–1678.
15. Kazakia GJ, Burghardt AJ, Cheung S, Majumdar S. Assessment of bone tissue mineralization by conventional x-ray microcomputed tomography: comparison with synchrotron radiation microcomputed tomography and ash measurements. Medical physics. 2008; 35(7):3170–3179. [PubMed: 18697542]
16. Morgan EF, Keaveny TM. Dependence of yield strain of human trabecular bone on anatomic site. J Biomech. 2001; 34(5):569–577. [PubMed: 11311697]
17. Burghardt AJ, Kazakia GJ, Laib A, Majumdar S. Quantitative assessment of bone tissue mineralization with polychromatic micro-computed tomography. Calcif Tissue Int. 2008; 83(2): 129–138. [PubMed: 18685797]
18. Zhou B, Liu XS, Wang J, Lu XL, Fields AJ, Guo XE. Dependence of mechanical properties of trabecular bone on plate–rod microstructure determined by individual trabecula segmentation (ITS). Journal of biomechanics. 2014; 47(3):702–708. [PubMed: 24360196]
19. Saha PK, Chaudhuri BB. 3D digital topology under binary transformation with applications. Comput Vis Image Underst. 1996; 63(3):418–429.
20. Saha PK, Chaudhuri BB, Dutta D, Majumder DD. A new shape preserving parallel thinning algorithm for 3D digital images. Pattern Recogn. 1997; 30(12):1939–1955.
21. Bayraktar HH, Morgan EF, Niebur GL, Morris GE, Wong EK, Keaveny TM. Comparison of the elastic and yield properties of human femoral trabecular and cortical bone tissue. Journal of biomechanics. 2004; 37(1):27–35. [PubMed: 14672565]
22. Bourne BC, van der Meulen MC. Finite element models predict cancellous apparent modulus when tissue modulus is scaled from specimen CT-attenuation. Journal of biomechanics. 2004; 37(5): 613–621. [PubMed: 15046990]
23. Busse B, Hahn M, Soltau M, Zustin J, Puschel K, Duda GN, Amling M. Increased calcium content and inhomogeneity of mineralization render bone toughness in osteoporosis: mineralization, morphology and biomechanics of human single trabeculae. Bone. 2009; 45(6):1034–1043. [PubMed: 19679206]
24. Liu XS, Cohen A, Shane E, Stein E, Rogers H, Kokolus SL, Yin PT, McMahon DJ, Lappe JM, Recker RR, Guo XE. Individual trabeculae segmentation (ITS)–based morphological analysis of high-resolution peripheral quantitative computed tomography images detects abnormal trabecular plate and rod microarchitecture in premenopausal women with idiopathic osteoporosis. Journal of Bone and Mineral Research. 2010; 25(7):1496–1505. [PubMed: 20200967]
25. Gross T, Pahr DH, Peyrin F, Zysset PK. Mineral heterogeneity has a minor influence on the apparent elastic properties of human cancellous bone: a SRmuCT-based finite element study. Computer methods in biomechanics and biomedical engineering. 2012; 15(11):1137–1144. [PubMed: 22263706]
26. Dede AD, Tournis S, Dontas I, Trovas G. Type 2 diabetes mellitus and fracture risk. Metabolism: clinical and experimental. 2014; 63(12):1480–1490. [PubMed: 25284729]
27. Nickolas TL, Leonard MB, Shane E. Chronic kidney disease and bone fracture: a growing concern. Kidney international. 2008; 74(6):721–731. [PubMed: 18563052]
28. Nishiyama KK, Cohen A, Young P, Wang J, Lappe JM, Guo XE, Dempster DW, Recker RR, Shane E. Teriparatide increases strength of the peripheral skeleton in premenopausal women with idiopathic osteoporosis: a pilot HR-pQCT study. The Journal of clinical endocrinology and metabolism. 2014; 99(7):2418–2425. [PubMed: 24684466]
29. Ross RD, Edwards LH, Acerbo AS, Ominsky MS, Virdi AS, Sena K, Miller LM, Sumner DR. Bone matrix quality after sclerostin antibody treatment. Journal of bone and mineral research : the official journal of the American Society for Bone and Mineral Research. 2014; 29(7):1597–1607.

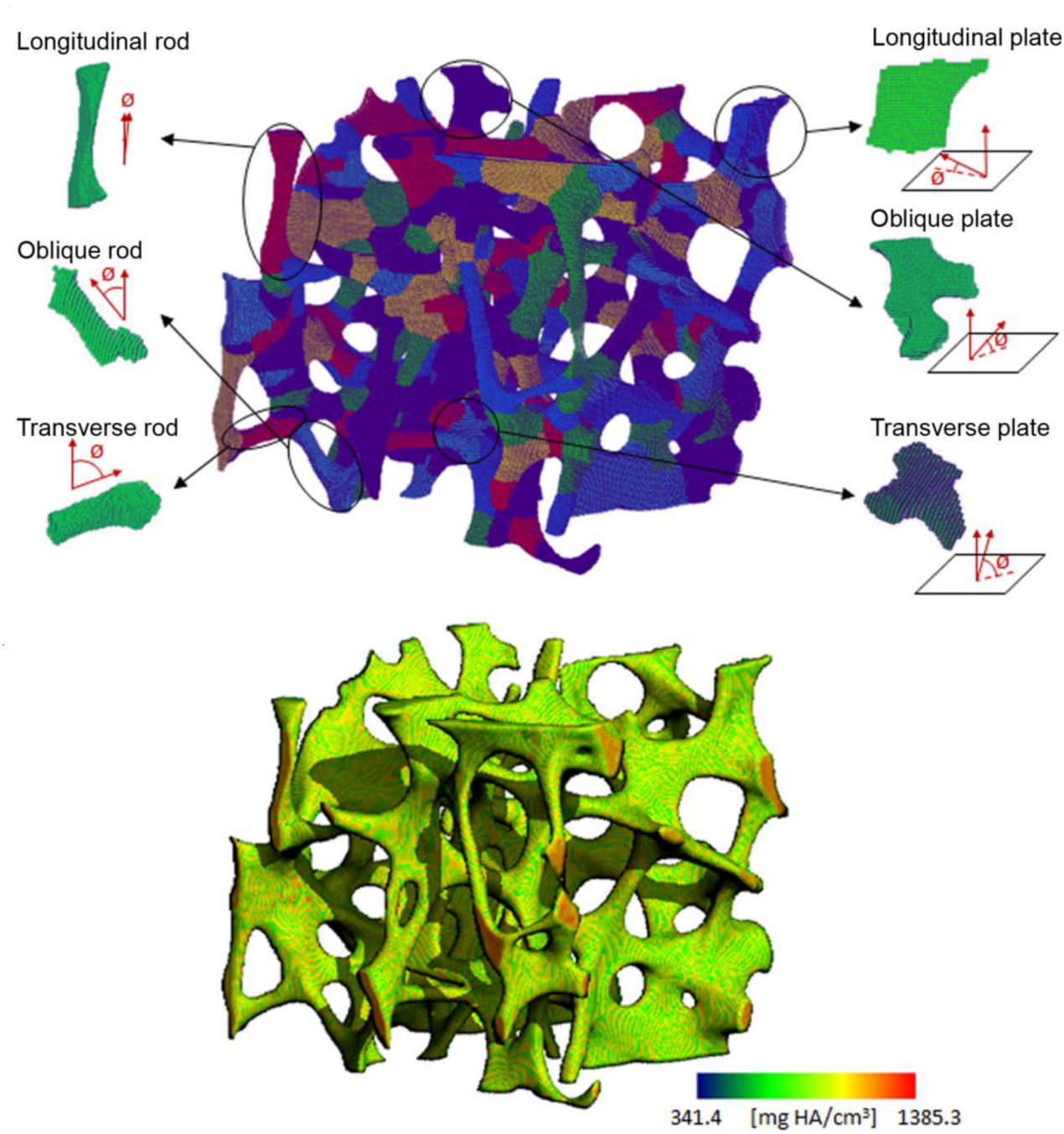

Figure 1.
Illustration of ITM analysis: (top) decomposition of trabecular microstructure into individual trabecular plates and rods along various orientations; (bottom) grayscale image of trabecular bone to be mapped to the segmented trabecular microstructure to quantify the TMD of individual plates and rods.

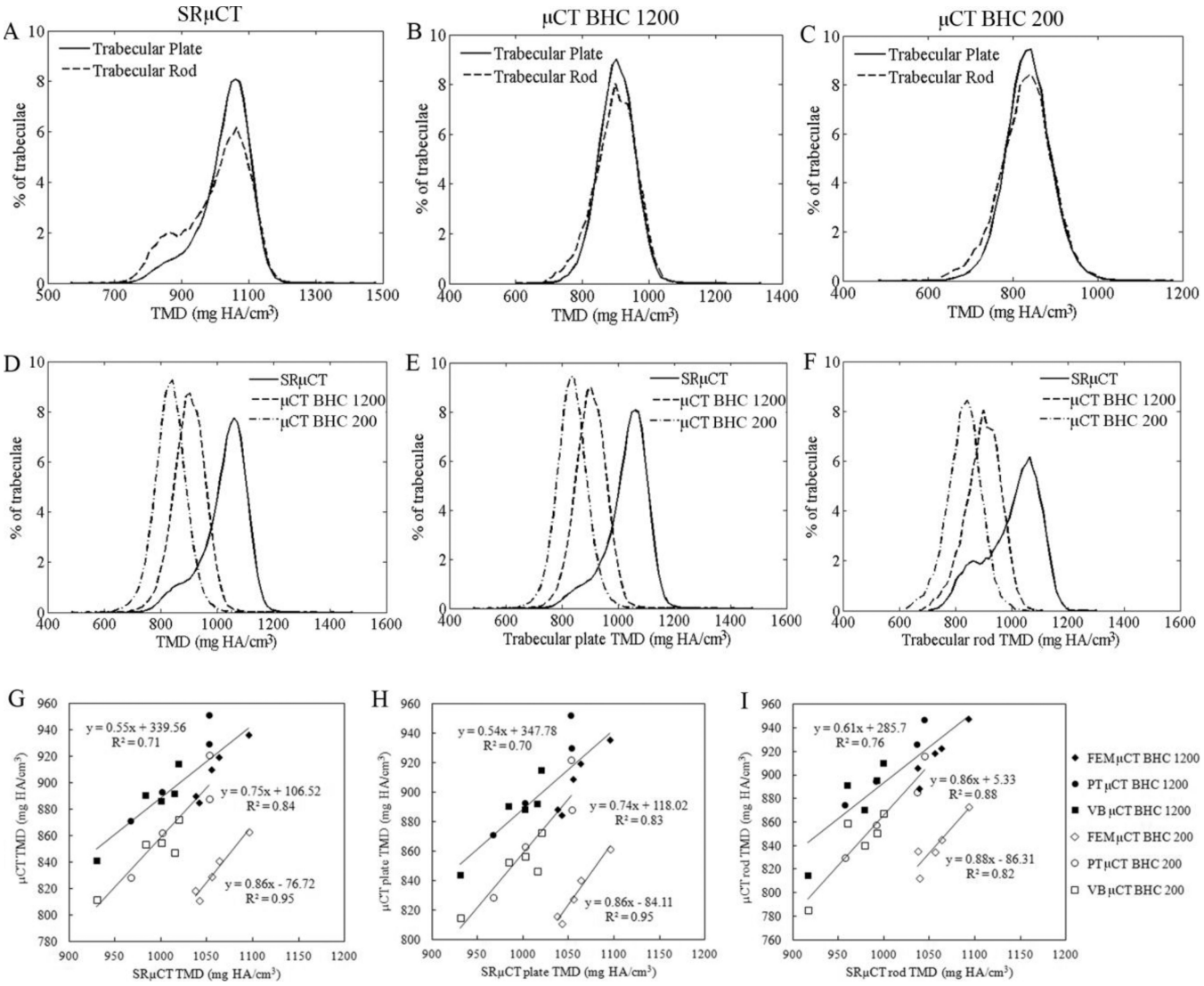

Figure 2.

(A~C) Measurements of trabecular plate and rod TMD distributions for the validation set by SRμCT, μCT with 1200, and 200 mg HA/cm^3 beam hardening corrections; (D~F) comparisons of TMD, pTMD, and rTMD assessments by SRμCT and μCT with 1200 and 200 mg HA/cm^3 beam hardening corrections; and (G~I) regressions of μCT and SRμCT TMD assessments of all trabeculae, trabecular plates, and rods.

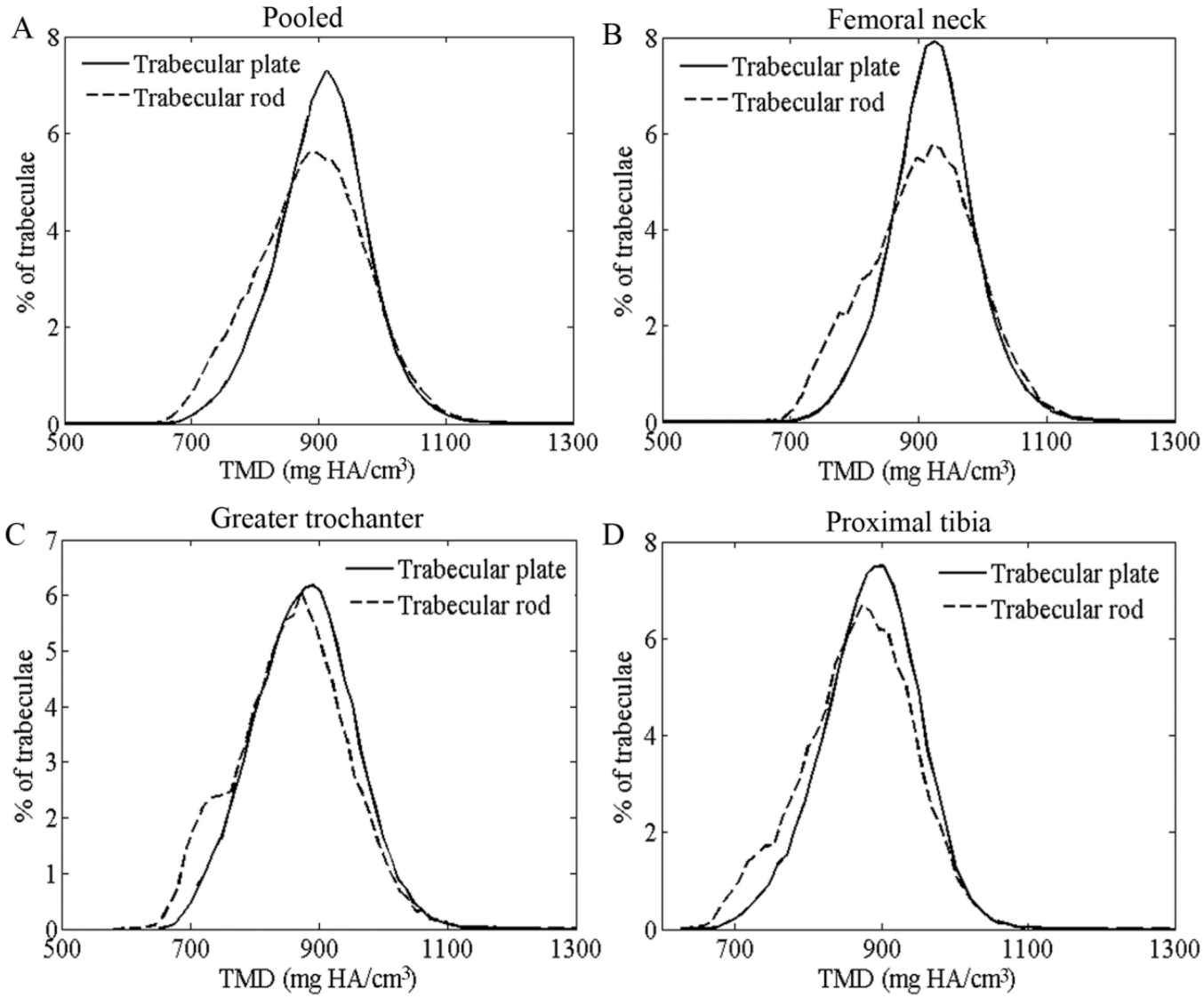

Figure 3.

Measurements of trabecular plate and rod TMD distributions for the experimental data set pooled from (A) three anatomic locations; (B) femoral neck; (C) greater trochanter; (D) proximal tibia.

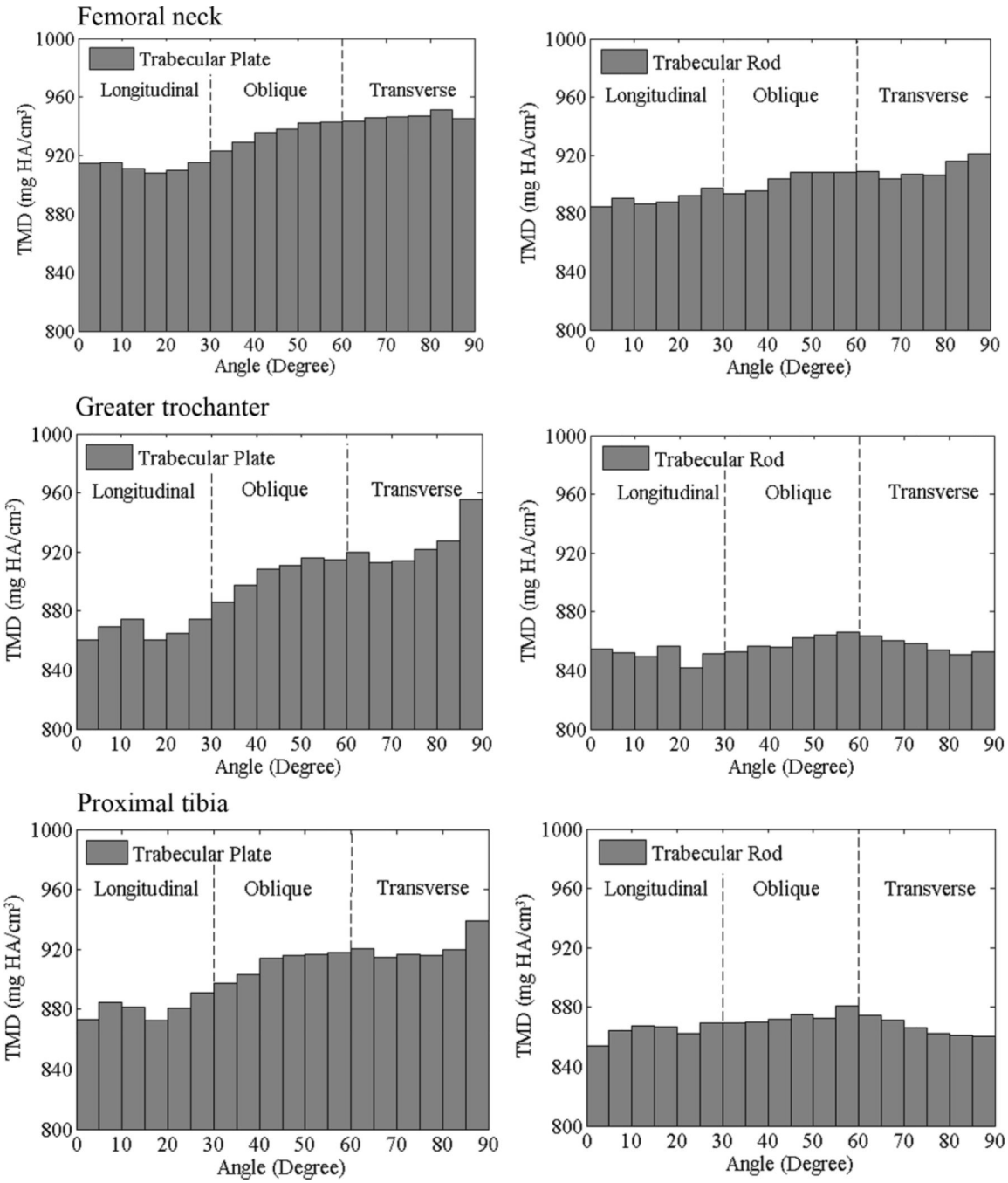

Figure 4.

Distributions of individual trabecula TMD along trabecular orientation from the longitudinal to transverse direction for trabecular plates (left column) and rods (right column) and for femoral neck (top), greater trochanter (middle), and proximal tibia (bottom).

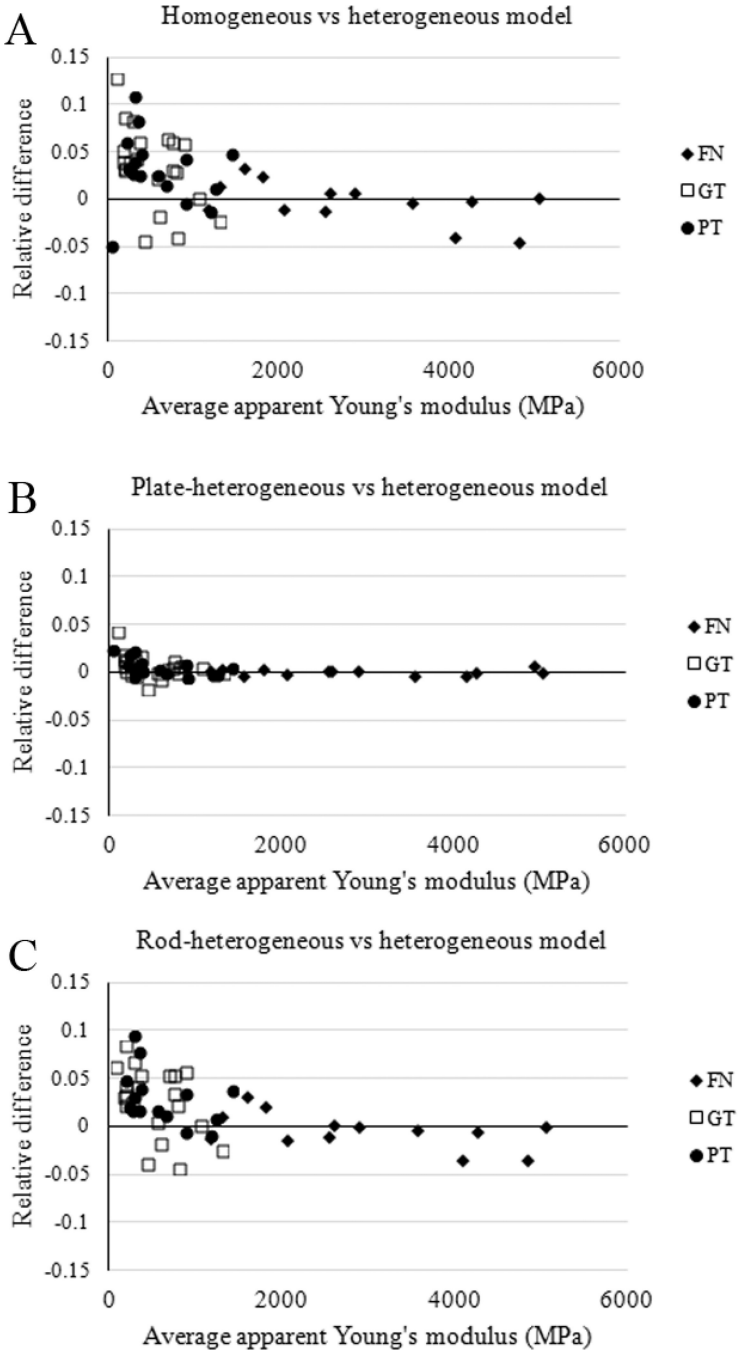

Figure 5.

Bland-Altman plots of the difference in apparent Young's modulus as predicted by (A) homogeneous *vs.* heterogeneous model, (B) plate-heterogeneous *vs.* heterogeneous model, and (C) rod-heterogeneous *vs.* heterogeneous model.

Table 1

Donor and sample information in the experimental set

Anatomic site	No. Specimens	No. Donors (male/female)	Age (year)	BV/TV
Proximal tibia	22	12 (11/1)	65±7	0.094±0.03
Femoral neck	20	13 (7/6)	72±15	0.28±0.10
Greater Trochanter	21	12 (8/4)	73±13	0.086±0.031

Table 2

TMD distribution parameters of trabecular plates and rods in the validation set (n=5, femoral head; n=5, vertebral body; n=4 proximal tibia)

TMD distribution parameters	Plate (Mean±SD)	Rod (Mean±SD)	p
SRμCT			
TMD_{MEAN} (mg HA/cm^3)	1006.90 ± 47.70	977.80 ± 54.01	**<0.001**
TMD_{PEAK} (mg HA/cm^3)	1033.72 ± 47.81	1012.71 ± 62.08	**0.007**
TMD_{WIDTH} (mg HA/cm^3)	95.68 ± 17.17	124.85 ± 38.97	**0.003**
TMD_{LOW} (%)	5.57 ± 4.95	14.06 ± 9.50	**<0.001**
TMD_{HIGH} (%)	3.09 ± 5.14	3.43 ± 5.55	0.15
μCT BHC 1200			
TMD_{MEAN} (mg HA/cm^3)	895.69 ± 28.67	885.43 ± 35.55	**0.006**
TMD_{PEAK} (mg HA/cm^3)	899.11 ± 32.57	895.12 ± 39.98	0.43
TMD_{WIDTH} (mg HA/cm^3)	102.05 ± 12.88	107.00 ± 24.70	0.44
TMD_{LOW} (%)	5.54 ± 4.76	12.66 ± 11.59	**0.005**
TMD_{HIGH} (%)	4.62 ± 4.59	5.34 ± 5.22	**0.03**
μCT BHC 200			
TMD_{MEAN} (mg HA/cm^3)	845.22 ± 30.93	834.44 ± 32.01	**0.004**
TMD_{PEAK} (mg HA/cm^3)	849.97 ± 34.58	844.93 ± 35.88	0.55
TMD_{WIDTH} (mg HA/cm^3)	100.73 ± 12.79	115.17 ± 31.53	0.07
TMD_{LOW} (%)	3.81 ± 2.88	8.90 ± 6.56	**0.002**
TMD_{HIGH} (%)	8.47 ± 12.09	8.55 ± 10.16	0.91

Table 3

TMD distribution parameters of trabecular plates and rods from PT, FN and GT in the experimental set. (p value of paired Student's *t* tests for plate- and rod-related parameters)

Variable	Plate Mean±SD	Rod Mean±SD	p
Pooled (n=63)			
TMD_{MEAN} (mg HA/cm^3)	891.66 ± 33.49[a]	871.54 ± 33.47[a]	**<0.001**
TMD_{PEAK} (mg HA/cm^3)	896.32 ± 36.30[a]	884.08 ± 43.56	**0.005**
TMD_{WIDTH} (mg HA/cm^3)	136.00 ± 32.32[c]	148.02 ± 41.97	**0.002**
TMD_{LOW} (%)	4.94 ± 4.86[d]	11.90 ± 8.15	**<0.001**
TMD_{HIGH} (%)	3.13 ± 6.44	2.98 ± 5.10	0.49
PT (n=22)			
TMD_{MEAN} (mg HA/cm^3)	883.77 ± 25.97	867.19 ± 27.76	**<0.001**
TMD_{PEAK} (mg HA/cm^3)	887.86 ± 25.67	882.20 ± 29.17	0.14
TMD_{WIDTH} (mg HA/cm^3)	126.98 ± 15.17	132.00 ± 24.64	0.32
TMD_{LOW} (%)	4.76 ± 4.63	10.93 ± 7.44	**<0.001**
TMD_{HIGH} (%)	1.28 ± 1.03	1.34 ± 1.47	0.75
GT (n=21)			
TMD_{MEAN} (mg HA/cm^3)	875.98 ± 29.26	857.39 ± 27.41	**<0.001**
TMD_{PEAK} (mg HA/cm^3)	878.15 ± 31.02	869.85 ± 37.52	0.38
TMD_{WIDTH} (mg HA/cm^3)	156.91 ± 41.94	158.79 ± 53.28	0.74
TMD_{LOW} (%)	8.40 ± 5.04	16.01 ± 9.07	**<0.001**
TMD_{HIGH} (%)	2.78 ± 3.31	2.49 ± 2.54	0.24
FN (n=20)			
TMD_{MEAN} (mg HA/cm^3)	916.81 ± 31.69	891.17 ± 36.92	**<0.001**
TMD_{PEAK} (mg HA/cm^3)	924.70 ± 35.54	901.08 ± 56.91	**0.007**
TMD_{WIDTH} (mg HA/cm^3)	123.95 ± 23.94	154.36 ± 40.25	**<0.001**
TMD_{LOW} (%)	1.51 ± 1.00	8.64 ± 6.19	**<0.001**
TMD_{HIGH} (%)	5.53 ± 10.61	5.31 ± 8.15	0.72

ANOVA suggested:

[a] FN different from PT and GT;

[b] PT different from FN and GT;

[c] GT different from FN and PT;

[d] any two sites different from each other